Annals of Biomedical Engineering, Vol. 37, No. 3, March 2009 (© 2008) pp. 503–515
DOI: 10.1007/s10439-008-9627-4

MRI-Based CFD Analysis of Flow in a Human Left Ventricle: Methodology and Application to a Healthy Heart

TORSTEN SCHENKEL,[1] MAURO MALVE,[1] MICHAEL REIK,[1] MICHAEL MARKL,[2] BERND JUNG,[2] and HERBERT OERTEL[1]

[1]Institute of Fluid Mechanics, University of Karlsruhe, Karlsruhe, Germany; and [2]Department of Diagnostic Radiology, University Hospital Freiburg, Freiburg, Germany

(*Received 15 June 2007; accepted 16 December 2008; published online 6 January 2009*)

Abstract—A three-dimensional computational fluid dynamics (CFD) method has been developed to simulate the flow in a pumping left ventricle. The proposed method uses magnetic resonance imaging (MRI) technology to provide a patient specific, time dependent geometry of the ventricle to be simulated. Standard clinical imaging procedures were used in this study. A two-dimensional time-dependent orifice representation of the heart valves was used. The location and size of the valves is estimated based on additional long axis images through the valves. A semi-automatic grid generator was created to generate the calculation grid. Since the time resolution of the MR scans does not fit the requirements of the CFD calculations a third order bezier approximation scheme was developed to realize a smooth wall boundary and grid movement. The calculation was performed by a Navier–Stokes solver using the arbitrary Lagrange–Euler (ALE) formulation. Results show that during diastole, blood flow through the mitral valve forms an asymmetric jet, leading to an asymmetric development of the initial vortex ring. These flow features are in reasonable agreement with *in vivo* measurements but also show an extremely high sensitivity to the boundary conditions imposed at the inflow. Changes in the atrial representation severely alter the resulting flow field. These shortcomings will have to be addressed in further studies, possibly by inclusion of the real atrial geometry, and imply additional requirements for the clinical imaging processes.

Keywords—Patient specific, Modeling, MRI, Computational fluid dynamics, In vivo, MRI flux, Magnetic resonance imaging, Ventricle, Blood flow simulation.

INTRODUCTION

With cardiovascular diseases being the number one cause of death in the western world, great scientific effort is put into understanding this organ's structure and function. Starting from a microscopic level, holistic approaches have highly increased our knowledge about the hearts function as a muscle,[14,27,29] but little about its function as a pump.

The heart is a complex system whose function is not only governed by fluid-dynamics, but also by structural-dynamics and electro-dynamics. The efforts to create a holistic fully coupled model of the heart's function are not yet applicable on a clinical patient specific base. With the aim of clinical application a simplified, separated approach is suggested.

In recent years, there have been growing efforts and successes in three dimensional CFD simulation and high resolution 3D measurements of the motion and blood flow of the heart. Experimental studies based on Echo-Doppler or Phase-Mapping MRI measurements[10,16,17] as well as simulations on generic models[6,9,26,30] have provided insight into the complex asymmetric vortex formation at the mitral orifice. The asymmetry in these vortices is considered a crucial feature in the ventricular flow pattern. Based on the slightly elongated, basically ellipsoidal geometry of the ventricle an efficient flow with low losses has to minimize the overall acceleration and deceleration during the pumping cycle as well as overall energy dissipation. This can be achieved by the asymmetric ring vortex pattern that has been observed experimentally as well as numerically. While earlier works suggested that the asymmetry was induced by the inner mitral valve tip, Pedrizzetti and Domenichini[9,30] have shown that the vortex is born from the inlet jet shear layer that rolls up due to the viscous forces exerted onto the jet core by the initially resting fluid in the ventricle and corresponds to the well known ring vortex behind an annular orifice. Furthermore their results suggest that the asymmetric vortex growth is the result of the lateral displacement of the mitral valve from the ventricle axis.

Address correspondence to Torsten Schenkel, Institute of Fluid Mechanics, University of Karlsruhe, Karlsruhe, Germany. Electronic mail: torsten.schenkel@kit.edu

From a fluid dynamicists point of view the numerical models of the heart can roughly be divided into two types: firstly, the models which take into account the interaction between the fluid flow and the motion driving it: the fluid–structure interaction (FSI) models, including fictitious domain models[18,19,23,24,33,41] and coupled FSI models.[7,42–45] And secondly those that take the movement of the inner ventricular wall as a boundary condition: the prescribed geometry models.[3–5,21,35,36,38,40] Both models cannot be considered as alternatives to each other but as approaches in their own right.

While a coupled FSI approach is promising for future work and is pursued in parallel work,[8] the numerical schemes necessary to simulate the coupled systems are not yet fully developed and tested. For a clinical *status quo* analysis and evaluation of intraventricular flow a prescribed geometry model is better suited. This statement is based on the assumption that the effect of forces exerted by the heart muscle onto the fluid are much larger than the effect of wall forces exerted by the fluid back onto the muscle tissue. Based on the results of this study, Baccani *et al.*[3–5] and Saber *et al.*[35,36] there is no evidence that this assumption is not true for the systole and comparison with FSI simulations[8] shows similar flow patterns also for diastole.

We present a prescribed geometry approach based on patient specific MR data, which can be acquired using standard clinical imaging procedures and thus will not put additional stress on the subject. The method is independent but similar in approach to Saber *et al.*[35,36] but includes an advanced valve model where Saber *et al.*[35,36] uses simple pressure boundaries. As it was shown in Long *et al.*[21] the intra ventricular flow is highly sensitive to changes in simple pressure boundaries.

The method will be part of a framework for heart simulation (KAHMO, Karlsruhe Heart Model). A functional method to simulate and classify the overall flow structure can help the clinical cardiologist to decide, if surgery is necessary and which surgical method is applicable.

METHODS

Magnetic Resonance Imaging

All experiments were carried out on a Siemens Sonata 3 T system (TRIO, Siemens Medical Solutions, Erlangen, Germany, gradient performance: 40 mT/m in 200 s) using an eight-element phased array body coil.

Two different sets of MRI data have been acquired. One intensity scan for reconstruction of the ventricular geometry and one phase coded flux scan for mapping of the blood flow.

Geometry Measurements

ECG-gated CINE images are acquired using k-space segmented scan procedures usually based on gradient echo or segmented EPI pulse sequences.[1,13,20]

Image acquisition was performed with a retrospectively cardiac gated balanced rf-spoiled gradient echo sequence with $TE/TR = 2.8/3.4$ ms and a bandwidth of 450 Hz/pix. The flip angle was set to 15°. With 9 echoes acquired per cardiac frame and a data matrix of 126×192 (325×400 mm^2 FOV, pixel size 2.6×2.1 mm^2), a temporal resolution of 30.6 ms was achieved. Images were acquired in a short axis orientation with a slice thickness of 5 mm. The entire heart including left and right ventricles and atria was covered with gapless slices from basis to apex. To eliminate breathing artifacts, all measurements were performed during breath-holding on a slice-by-slice basis.

Flux Measurements

In addition to the geometry measurements velocity phase mapping scans[2,31,34] have been taken for one characteristic slice.

2D MR velocity mapping data were acquired using an rf-spoiled gradient echo sequence with interleaved 3-directional flow velocity encoding. Measurements were performed during breath-holding and prospectively gated to the ECG cycle. Further imaging parameters were as follows: flip angle = 15°, venc = 150 cm/s, $TE = 3.4$ ms, $TR = 6.4$ ms, temporal resolution 63.6 ms, band width of 650 Hz/pix. MR measurements were performed in a four-chamber view (rectangular FOV = (300×400) mm^2) with a slice thickness of 8 mm with an in-plane spatial resolution of (2.0×1.6) mm^2.

Segmentation

The high contrast MR images were used to determine the three dimensional shape of the left ventricle endocardium for each scan time. Drawing these contours manually in every slice image is a very time consuming and tedious task. To ensure a consistent and accurate segmentation a semi-automatic procedure is employed. The segmentation was performed by Fraunhofer FIT using an in house tool using the Live Wire or Intelligent Scissors method[25] based on the graph theoretical Dijkstra algorithm. The method is able to determine the endocardium contour in an MR slice from few seed points without the need to draw the contour exactly.

Contours in spatially or temporarily adjacent slices usually differ only slightly. This can be used to reduce overall segmentation time and the need for interaction.

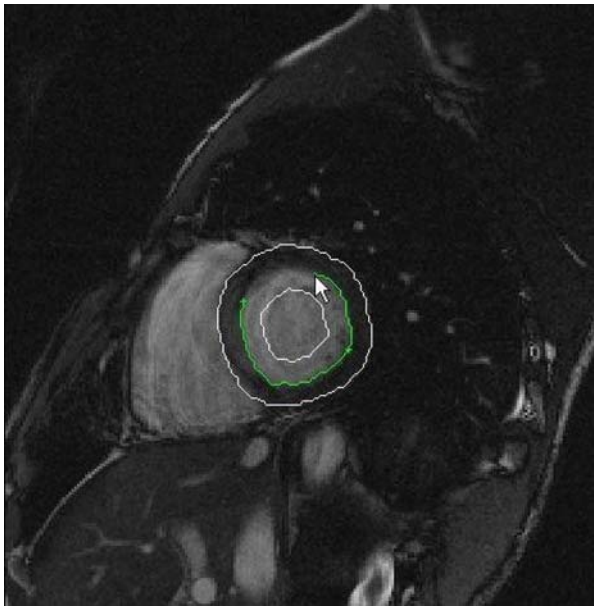

FIGURE 1. Segmentation of the endocardium wall of the left ventricle (green) from a short axis slice using the Live Wire algorithm.

If a neighboring contour for a slice that is to be segmented exists, a distance image of the adjoined contour is calculated.[37] Cost calculation in the new slice is then reduced to a local search area defined by a maximum distance from the neighboring contour (see Fig. 1). Path costs are modified based on the neighboring contours.[25,37] This is partially automized such that contours are propagated spatially (from apex to base) and temporarily (from end diastole to end systole) onto neighboring slices and the global minimum of the cost function in the search area around the propagated contour is used as the segmented contour on the new slice.[12,15] Usually the neighboring contours have only to be checked for correctness. Corrections to single contours are automatically propagated further, so propagating errors can easily be corrected.

Natural contours in medical imaging seldom have sharp angles or bends. Segmentation algorithms often include a smoothness condition. The life wire algorithm does not have such a condition. Thus very sharp and ragged contours can be calculated. Following[39] the graph is modified such that only edges forming a maximum angle of 45° with the previous edge on the path are considered for calculation. This reduces the local curvature of the segmented contour.

The valves cannot be segmented as accurately as the geometry of the ventricle endocardium. Most MR measurements lack sufficient resolution in the valve areas to segment enough base points for a description of the valve position and shape. To increase the number of base points on the valve ring additional long axis slices are defined which intersect with the valve ring in at least 4 positions. The intersection points on the valve ring are segmented manually. Additionally the angle between the valve rings is measured in the long axis slices. Using this information the valve ring position for the aortic and the mitral valve is reconstructed.

Since the MRI data did not have any information on tissue velocity the moving wall boundary condition has to be derived from the change in position between two following scans. This results in a high error with regard to local radial velocities and a complete neglection of tangential velocities. Due to the nature of accelerated or decelerated flow the friction boundary layers are expected to be very small and the effect of the wall velocity on the bulk flow to be negligible. The change of volume can be estimated within a range of ±9% for a very high contrast image as was used in this study.

Numerical Method

The simulation of the fluid flow is performed using the finite volume method in the arbitrary Lagrange–Euler (ALE) formulation for moving grids as implemented in the commercially available Star-CD solver (Computational Dynamics Ltd., London).

For an arbitrary volume V with surface S moving with local surface velocity $\mathbf{v}_S$ the integral form is as follows

$$\frac{\partial}{\partial t}\int_V \rho dV + \int_S \rho(\mathbf{v}-\mathbf{v}_S)\cdot\mathbf{n}dS = 0 \tag{1}$$

$$\frac{\partial}{\partial t}\int_V \rho\mathbf{v}dV + \int_S (\rho\mathbf{v}(\mathbf{v}-\mathbf{v}_S)+p\mathbf{I}-\tau)\cdot\mathbf{n}dS = 0 \tag{2}$$

where ρ is the fluid density, $\mathbf{v}$ the fluid velocity vector in the fixed coordinate system, $\mathbf{v}_S$ the velocity vector of the boundary S of the control volume V, $\mathbf{n}$ the normal outward unity vector of this boundary, p the pressure, $\mathbf{I}$ the unit tensor and τ the viscous stress tensor.

Though blood is a non-Newtonian fluid the viscous stress tensor is still being modeled by:

$$\tau_{ij} = \mu_{\text{eff}}\left(\frac{\partial u_i}{\partial x_j}+\frac{\partial u_j}{\partial x_i}\right) \tag{3}$$

where μ_{eff} is the local viscosity, which is adapted to the local shear rate (see section "Viscous Model").

V in Eqs. (1) and (2) is an arbitrary volume with surface S. The approximation schemes used in this work are a modified linear spatial and a temporal time stepping scheme (MARS and Euler implicit,[11] respectively). The resulting algebraic equation system is solved using the implicit PISO algorithm.

Viscous Model

The rheology of blood is very complex. Several rheological models on different levels are described in literature. The most complex models are taking into account the time history of the corpuscle agglomerates. Since the typical aggregation time is about one order of magnitude higher than the heart cycle time while the disaggregation is virtually instantaneous, a Eulerian model that modifies the viscosity based solely on the shear rate is used. The model used is based on the Cross model with modifications by Perktold.[32] For a three dimensional flow the viscosity–shear relation is:

$$\frac{\mu_{(|II_D|)} - \mu_\infty}{\mu_0 - \mu_\infty} = \frac{1}{\left(1 + \left(\lambda \cdot 2\sqrt{|II_D|}\right)^b\right)^a} \qquad (4)$$

with $\mu_0 = 0.135$ Pa s and $\mu_\infty = 0.03$ Pa s, the asymptotic viscosity for low and high shear rates, respectively; II_D, the second invariant of the shear rate tensor; $\lambda = 0.5$ s, a time constant (adapted for a change rate of 2 Hz) and the model constants $a = 0.3$, $b = 1.7$. Figure 2 shows the viscosity over the shear rate. The typical shear rate that was observed in our simulation ranges from 5 to 100 s^{-1}. The volume averaged viscosity varies between 5 to 6 mPa s.

Grid Generation and Movement

The presented model is a prescribed geometry model using a moving grid without modification of grid topology. Simulation is performed in a discontinuous time stepping fashion, i.e. the solution for each time step is calculated on a new grid, surface velocities for the ALE formulation are calculated from the differences between the current and the former grid.

For each segmented geometry a separate grid has to be generated which is topologically identical to all other grids. This is achieved by using a block structured hexahedral type grid. A semiautomatic grid generation technique was developed especially for this study. For each segmented endocardium geometry a tubelike base grid is projected onto the segmented surface giving identical vertex distributions adapted to the individual geometry. These vertices describe splines which together with the respective splines for the valve ring form the basis for the grid topology. The grid topology consists of two so-called O- or Butterfly-Grids for the inlet and outlet tracts which are combined to form the intraventricular grid. Figure 3 shows the grid for the ventricle and the block topology of the inlet and outlet and the intraventricular grid. Grid dependency studies performed for topologically identical grids with cell numbers ranging from 20,000 to 500,000 show that the global flow features do not change for cell numbers above 100,000 even if the vortex breakup shows more and more details as spatial and temporal resolution is increased. While the grid moves the quality was monitored and simulation stopped when grid quality fell below the threshold of maximum face warp angle of 50°. For high cell numbers >400,000 the grid quality could not be kept during the grid movement, results were therefore not used in the comparison. Based on this a grid size of 100,000 is sufficient to capture the global flow structure with reasonable effort. It has to be noted, that this rather coarse grid is not suitable to fully resolve the vortex breakup that occurs in the ventricle, but filters the small scales. To resolve all scales of vortices a much finer grid would be needed.

The temporal resolution of the MRI data is too rough for the numerical simulation. Therefore intermediate grids have to be calculated from the base grids at the scan times. For the given scan resolution of 17 grids over one heart cycle 50 intermediate steps between the 17 reconstruction grids are needed for the used grid to keep the flow and grid Courant numbers close to unity resulting in 850 timesteps for one cardiac cycle. The intermediate grids can be calculated by interpolation or approximation methods. Former studies with linear interpolation of the grid's movement showed high discontinuities in the pressure solution due to the resulting discontinuities in grid acceleration. Higher order interpolation splines on the other hand involve the solution of an additional equation system for each vertex, adding significantly to the overall simulation cost. To alleviate these issues a third order Bezier-Spline approximation method was used which is twice continuously differentiable. This approximation curve can be calculated independently for each vertex from the positions of each vertex in the base grids. The position of each vertex moves in time according to Eq. (5):

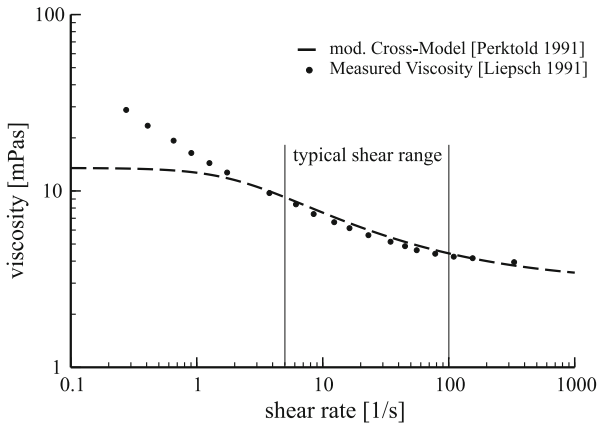

FIGURE 2. Blood viscosity over shear rate.

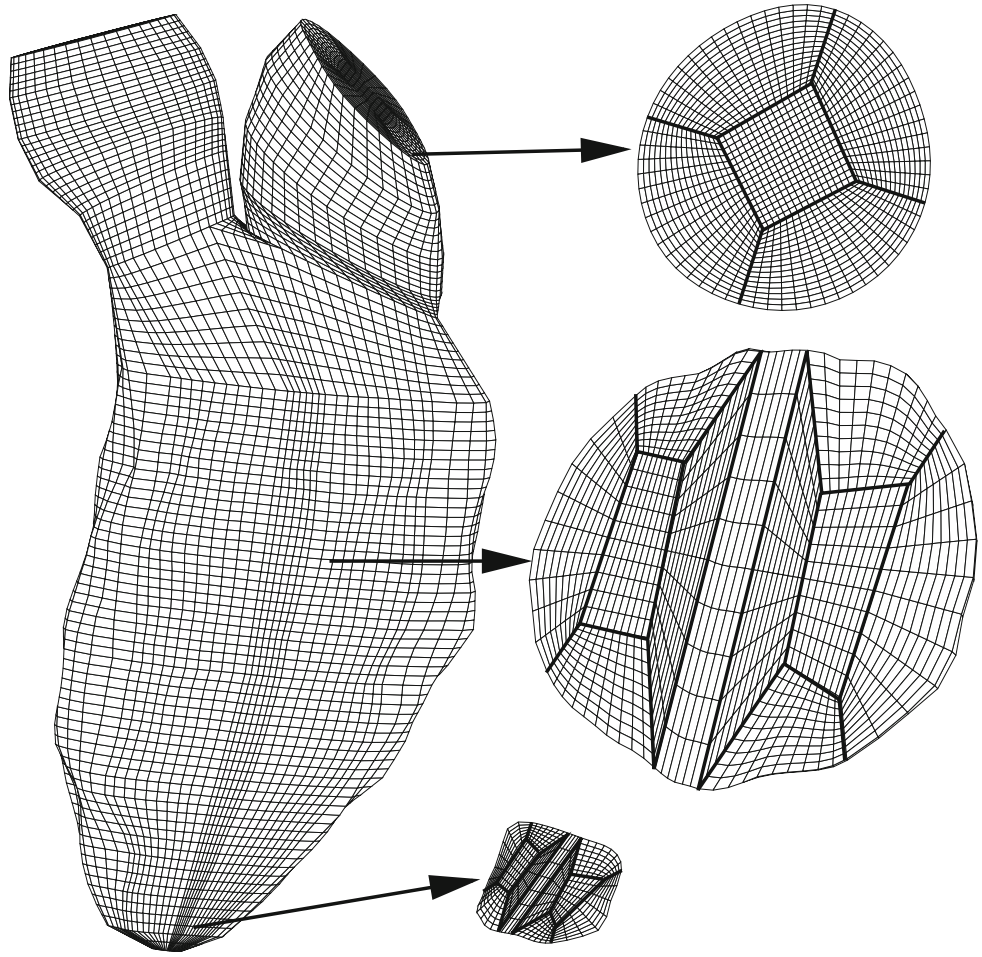

FIGURE 3. Grid topology for the ventricle, inlet/outlet and the intraventricular grid at base and apex.

$$\mathbf{x}_i(t') = (1-t')^3 \cdot \mathbf{b}_{0,i} + 3 \cdot (1-t')^2 \cdot t \cdot \mathbf{b}_{1,i} + 3 \cdot (1-t') \cdot t'^2 \cdot \mathbf{b}_{2,i} + t'^3 \cdot \mathbf{b}_{3,i} \quad (5)$$

with the Bezier points:

$$\begin{aligned} \mathbf{b}_{0,i} &= \frac{1}{6}(\mathbf{V}_{i-1} + 4\mathbf{V}_i + \mathbf{V}_{i+1}) \\ \mathbf{b}_{1,i} &= \frac{1}{3}(2\mathbf{V}_i + \mathbf{V}_{i+1}) \\ \mathbf{b}_{2,i} &= \frac{1}{3}(\mathbf{V}_i + 2\mathbf{V}_{i+1}) \\ \mathbf{b}_{3,i} &= \frac{1}{6}(\mathbf{V}_i + 4\mathbf{V}_{i+1} + \mathbf{V}_{i+2}) \end{aligned} \quad (6)$$

and $t' \in [0,1]$ for each of the 17 scan time intervals.

Figure 4 shows the resulting trajectory in comparison with the linear polygonal trajectory. It can be shown that a higher order bezier spline represents the fixed points V_n with lower fidelity than a lower order approximation and will never meet the exact geometry given for the 17 segmented measurements. Figure 5 shows the approximated relative ventricular volume (line) over time (related to end diastolic volume V_d) compared with the volume of the base grids (dots) for the segmented geometry. The scale at the

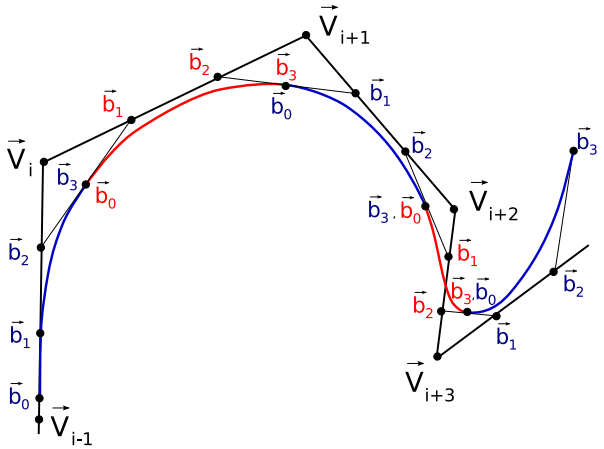

FIGURE 4. Third order Bezier trajectory of one grid vertex. V_i is the position of the vertex at the fixed grid time i, b_n are the Bezier points. In the simulation each vertex is moved along the resulting Bezier spline.

time or phase axis corresponds to the 12 phases measured in the MRI flux measurements used in the validation (see section "Comparison of Simulated and Measured Intraventricular Flow Patterns"). The exact positions in the base grids are only approximated by this approach, slightly altering the base geometry, but approximation errors are well within the segmentation error width of ±9% and are therefore neglectable. The time step size can be adapted to the cell sizes.

Valve Representation

Since the position and time dependent shape of the valve leaflets were not extractable from the MRI scans and it was not possible to incorporate a moving valve leaflet in the grid topology, the valves were represented by a two dimensional planar model. The model plane is the anular plane defined as described above. Onto this plane a generic opening area is projected. In the current simulations the valve geometry could not be measured for the actual subject. The opening area is therefore derived from 3D echocardiographic scans of sound aortic and mitral valves as well as from anatomical literature and adapted to the size of the valve derived from the MRI scans.

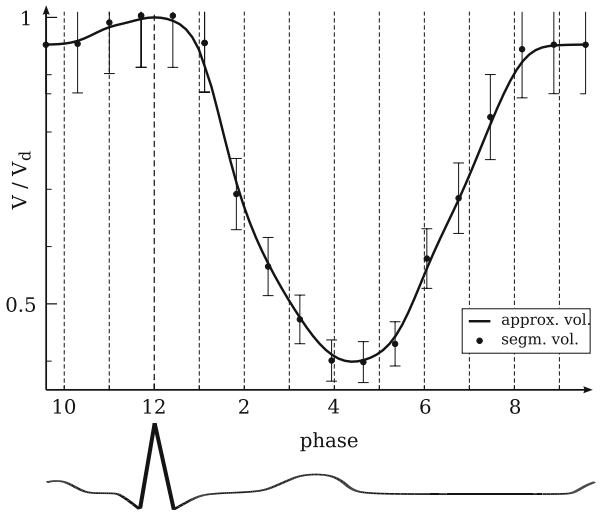

FIGURE 5. Approximated volume over time and segmented volumes. Segmented volumes are shown for the 17 MRI geometry measurements while the phases on the abscissa correspond to the 12 phases of the MRI flux measurement.

Numerically the valves are represented by a temporally and spatially variable pressure drop, realized by so-called "baffle" boundary conditions. The pressure drop is varied from infinite (closed valve area) to zero (open valve area). An intermediate pressure drop is defined for the border of the opening area, to smoothen the resulting jet profile in the same way as the three dimensional valve geometry does. By adaption of the intermediate pressure drop coefficient the evolving jet can be controlled such that the evolving velocity profile can be adapted to profiles measured in Echo- or MR-Flux measurements. If a measured velocity profile is available from an *in vivo* measurement the model parameters can be adapted such that the simulated velocity profile at the valve can be fitted to the measured one.

Figure 6 shows the opening process of the mitral and aortic valve model over 4 time steps, black is infinite, white is zero pressure drop, gray are the intermediate areas.

This valve model is neglecting any effects the mitral valve leaflets might have on the flow. A matter which is a point of vivid discussion in literature.[4,9,16,17] On the one hand the valve leaflets are very subtle and thus likely to orient themselves along the shear surfaces evolving in the flow. On the other hand the anterior leaflet of the mitral valve is located about one third from the central axis of the ventricle in front of the aortic outflow tract blocking this area from the flow. The effect of these facts on the overall flow structure is still to be evaluated.

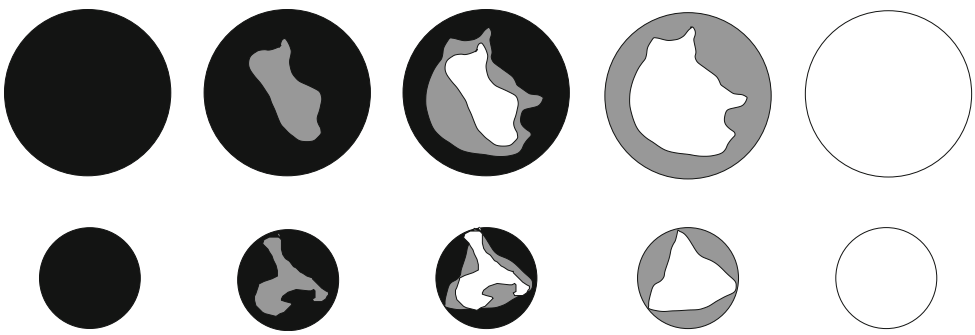

FIGURE 6. Opening sequence of projected heart valve model. Closed surfaces are black, free surfaces white. Gray denotes the transition area.

Boundary Conditions

The heart cannot be considered an isolated organ. The flow variables at the boundaries of the simulation area are not independent of the results of the simulation itself. It is therefore not possible to set realistic pressure boundary values at the mitral and aortic valve. Fortunately the incompressible balance equations for mass and momentum are not dependent on the pressure but on it's gradient and all pressures in the equation system can be treated as relative pressures.

Therefore a relative pressure boundary conditions was set at the respective open valve tract:

$$p = \text{const.}, \quad \frac{\partial \mathbf{v}}{\partial n} = 0.$$

The calculated pressures are to be evaluated in relation to the respective vessel pressure (pulmonary or aortic pressure). Since the systolic aortic pressure is typically more than 15,000 Pa higher than the pulmonary pressure the evaluation of the pressure-volume relation and by that the power output of the ventricle is only possible if these pressures are known from measurements or additional computation. This boundary condition dilemma is common to many biomechanical flow simulations. A one dimensional model for the human circulatory system, based on Naujokat and Kiencke,[28] which will be coupled with the three dimensional ventricle model, is currently developed, to provide realistic pressure boundary conditions.

To minimize the influence of the uniform pressure assumption on the intraventricular flow field the boundary location was moved upstream from the mitral and downstream from the aortic valve plane. This was done by inclusion of generic atrial and generic aortic geometries. As it was shown in Long *et al.*[21] and as will be shown in this work, the outflow and especially the inflow representation has a severe impact on the flow in the ventricle. Therefore future models will have to incorporate physiological atrial and aortic geometries to provide more realistic boundary conditions. These atrial and aortic geometries will have to be acquired by the MRI scans.

RESULTS

Integral Values: Volumes, Ejection Fraction

Figure 5 shows the normalized intra ventricular volume over time for the 17 segmented grids and the approximated volume of the moving simulation grid. For a heart rate of 79 min^{-1} the end diastolic volume is 166 ml, the end systolic volume 64 ml. This gives a stroke volume of 102 ml or an ejection fraction of 61.5% and a cardiac output of 8 l/min. These values are at the upper end of but well within the range typically measured in males.[22] It has to be mentioned here, that the fluid volumes evaluated from the MRI measurements include the volume taken up by the papillaries and trabeculae which are not resolved in the MRI scans. This effect slightly increases the measured volumes in our simulation. While this is of lesser importance when comparing ejection volumes and fractions between hearts, it might account for discrepancies in measured and simulated velocities across the valves.

In- and Outflow Velocities, Velocity Profiles

Comparison of in- and outflow velocity profiles in the valvular plane gives insight into the fidelity of the segmentation, the valve representation and the overall flow structure in the ventricle. The numerical results are compared with results from the MRI flux measurements. The flux measurements were available in one four-chamber view plane. The velocity profiles were extracted from the intersection lines between the measurement plane and the valvular planes. The extraction lines are displayed in Fig. 7. In Fig. 8, the simulated velocity profiles (lines) are compared with the measured velocities (dotted lines) for three points of time in the heart cycle: For the beginning (phase 6) and end of diastole (phase 8) the velocity profiles over the mitral valve are shown and for the systole (phase 1) we see velocities over the aortic valve. The phases correspond to the phases of the MRI flux measurement as shown in Fig. 5. In all cases the velocity component normal to the valve plane is shown.

The velocities were measured from MRI slices of 8 mm thickness. This will result in an averaging of velocities within that region. As a result, spatial averaging may occur which can result in underestimation of peak velocities.

FIGURE 7. Location of flux profiles. Dot denotes the origin.

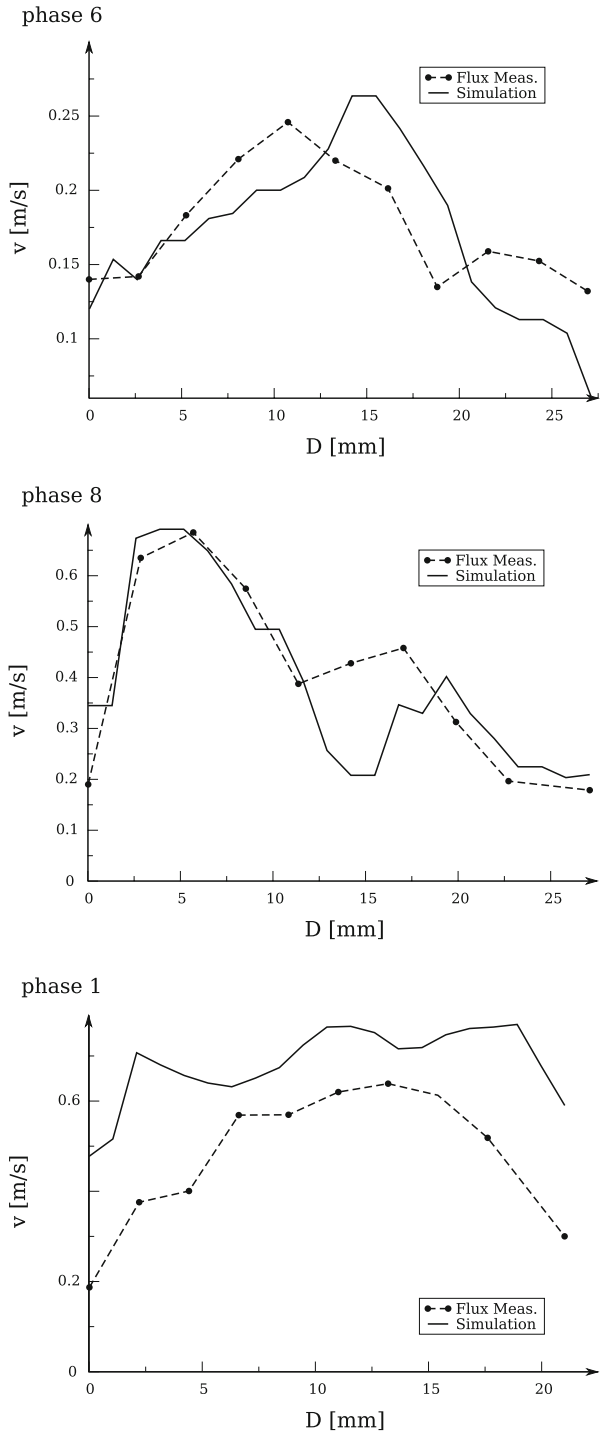

FIGURE 8. Velocity profiles over the mitral valve (beginning and mid-diastole: phase 6 and 8) and the aortic valve (beginning systole: phase 1).

The comparison shows good agreement with regard to magnitude and profile for the diastole. The kink in the velocity profile that develops in the later phase 8 is slightly more pronounced in the simulation. For the systolic phase the velocity magnitude is overpredicted in the simulation. This is due to an underestimation of the diameter of the aortic valve in the simulation. As said in section "Segmentation" the valve rings are segmented from limited data and therefore the uncertainty is rather high in the aortic valve area. In this case the segmented diameter for the aortic valve ring is 20 mm compared to the 22 mm measured from the 2-chamber long axis slice from the MRI flux measurement. This 10% discrepancy in diameter accounts for a 21% discrepancy in valve orifice area and velocity.

Comparison of Simulated and Measured Intraventricular Flow Patterns

For validation of the overall model *in vivo* data on the flow in the simulated ventricle is necessary. The *in vivo* flow data is taken from the MRI flux measurements which were performed in the four chamber plane as described in the section "Magnetic Resonance Imaging". Figure 9 panel A shows the flux measurement data. Velocity is color coded from blue (0 m/s) to red (0.7 m/s). In the beginning of diastole a ring vortex is formed behind the mitral orifice. During the course of the ventricular filling an asymmetry of the ring vortex and dominance of a clockwise overall rotation can be seen. For late ventricular filling the vortex breaks up partly.

Panel B of Fig. 9 shows the results from the simulation. The comparison between measured and simulated flow fields shows good overall agreement for the initial filling phase. The development of the vortex in the beginning of the diastole (A7 and B7) shows very good agreement. Later into the diastole (A8 and B8) the ring vortex grows asymmetrically with the left hand side growing stronger. This effect is more distinct in the measurement (A8) than in the simulation (B8). In the last third of the diastole (A9, B9), which corresponds to late ventricular filling the velocities are low and the measurement results do not show the clear distinction between the vortices as the simulation results, because the measurement threshold is constant over the cycle and the lower velocities cannot be resolved in the measurement.

It can be said that the simulation gives a fair representation of the initial filling of the ventricle. Further into the cycle discrepancies arise which probably originate from the high level of uncertainty in the representation of the actual geometry and boundary conditions in the numerical model. To overcome these limitations an *in vitro* validation experiment is planned where the geometry and boundary conditions can be accurately measured to engineering standards. Furthermore it has to be noted here that the development of the intraventricular flow is strongly dependent on the inflow conditions and therefore on the choice of upstream boundary conditions.

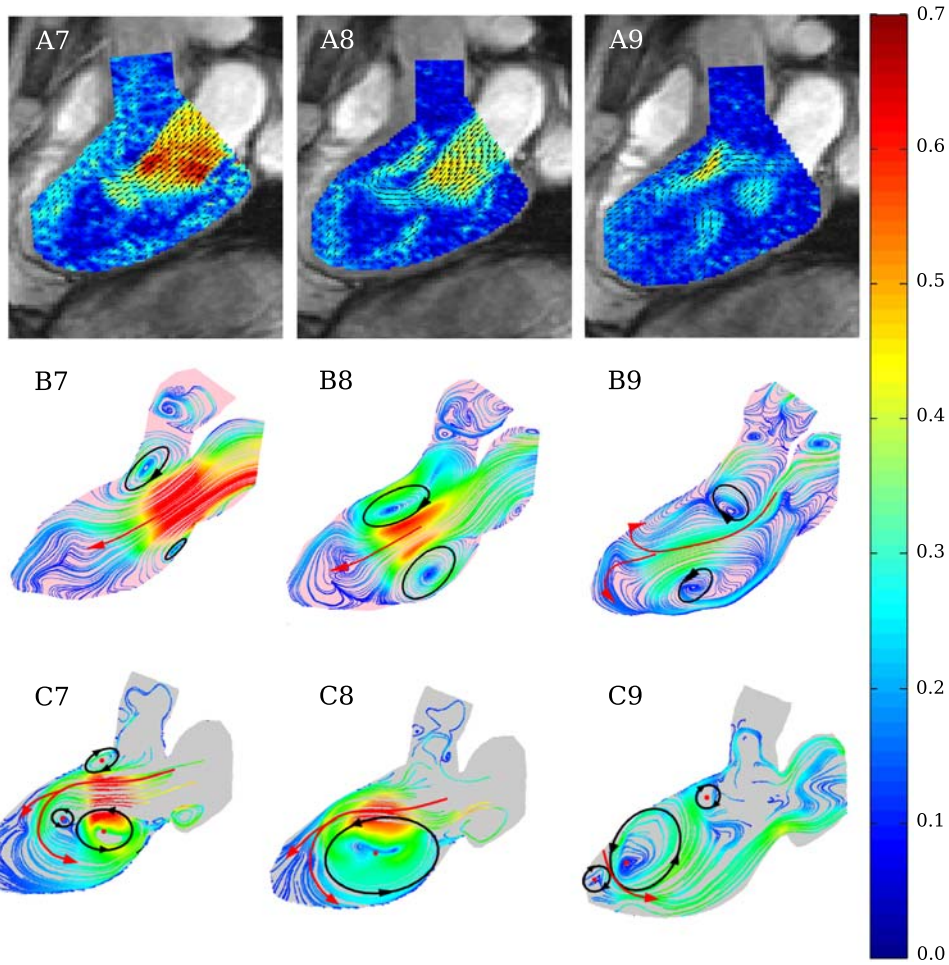

FIGURE 9. Sensitivity to inflow conditions. Lines show A: velocity contours and vectors, flux measurement, B: projected streamlines colored by velocity magnitude for the simulation with curved atrial geometry, C: projected streamlines colored by velocity magnitude for simulation with straight atrial geometry. Column numbers corresponds to the MRI flux phases (see Fig. 5).

Sensitivity to Inflow Conditions

Flows like the one in the human ventricle tend to be highly sensitive to changes in the boundary conditions. Since the geometry and boundary conditions are taken from clinical *in vivo* measurements we cannot clearly asses the differences between reality and numerical model. It is therefore interesting to check for sensitivity of the flow to small changes in the numerical models. In this case the model shows a high sensitivity to the conditions upstream of the mitral orifice.

The numerical model used here shows reasonable agreement with the flux measurement when compared quantitatively and qualitatively (Fig. 9B). But our experience and Long *et al.*[21] shows that the numerical representation of the atrial tract via the boundary conditions has a severe influence on the simulated flow field. While Long *et al.*[21] used pressure boundaries in the valvular plane, we tried to alleviate the problem by inclusion of a representation of the atrial geometry. The actual atrial geometry was not available, so a generic geometry was chosen in a way that the resulting circulation that is created in the atrium corresponded to the measured flow field.

To evaluate the influence of the atrium on the flow field in the ventricle we compared with the results obtained from an older numerical model which uses a different atrial representation that does not create a rotational flow through the atrium.

Panel C in Fig. 9 shows the results from this model. The flow pattern is distinctly different from the one observed in panels A and B. The asymmetry of the ring vortex is still governing the evolvement of the flow pattern, but the main flow direction is anti-clockwise. This result contradicts not only our own flux measurements, but also some published measurement results.[16,17] From this comparison it seems, that the atrial geometry plays a major role in the development of the intraventricular flow dynamics and that a realistic representation of the atrium might be necessary to correctly predict the intraventricular flow pattern. On

the other hand the inclusion of the atrial geometry increases the complexity of the model considerably and only shifts the boundary condition dilemma to the pulmonary vein. Further studies will have to show the feasibility of this approach.

Structure of Intraventricular Flow

The structure of the intraventricular flow is visualized in Fig. 10 by isosurfaces of λ_2 and streamlines. The contour field displays the velocity magnitude in the middle plane. In addition a schematic depiction is shown in Fig. 11. In the schematic picture the rear half of the vortex is shown, while in the λ_2 representation the front half is visible. In the beginning diastole blood enters the ventricle through the opening mitral valve. The resulting jet flow develops into a ring vortex (Fig. 10 phase 6). This initial vortex is born from the jet shear layer that is rolled up by viscous forces exerted from the resting fluid onto the jet core. This process is well known from accelerated flow through an anular orifice. Initially this ring vortex is nearly symmetrical and corresponds to the shape of the valvular opening. In a symmetrical vessel the ring vortex would keep traveling downstream in its symmetrical shape and finally dissipate—possibly deformed by instability waves. In our case the ring vortex originates from a laterally displaced orifice and enters an asymmetric ventricle. This leads to asymmetric growth of the ring vortex in the course of the diastole (Fig. 10 phase 8) and finally the vortex is tilted to fill the elongated shape of the ventricle (Fig. 10 phase 10).

The direction of the tilting is subject to boundary conditions, especially the inflow direction and the movement of the ventricle wall. In the left ventricle the tilting direction is clockwise such that the left side of the ring vortex stays in the upper part of the ventricle and grows to fill most of it's cavity and the right side dives into the apex and aids in flushing the tip of the ventricle.

This asymmetry in the vortex development seems to be crucial for the function of the ventricle, since without it the elongated shape cannot be flushed efficiently as a symmetrical ring vortex would stay in the wide part of the ventricular cavity leaving a stagnant area in the apex. The understanding of the relation between ventricular shape and motion and the asymmetry of the developing ring vortex is important for the understanding of the ventricular function as a whole.

At the beginning of the systole the vortical structures are only partly dissipated and most of the rotational energy pushes the blood toward the opening aortic valve (Fig. 10 phase 1).

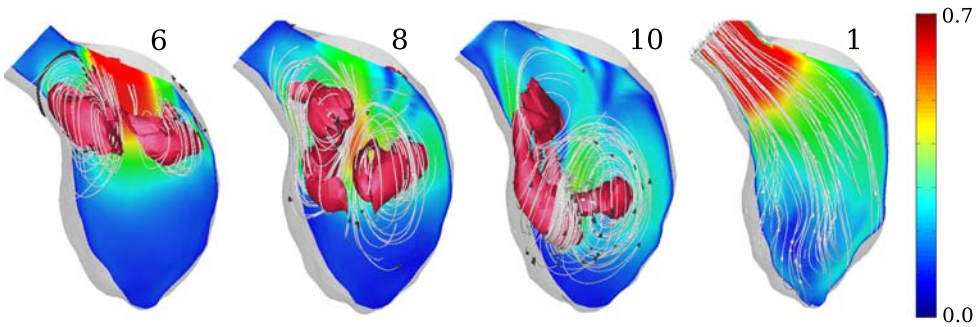

FIGURE 10. Flow structure in the left ventricle. Isosurface $\lambda_2 = -1000$ and 3D stream lines on velocity contour. Numbering corresponds to the MRI flux phases (see Fig. 5).

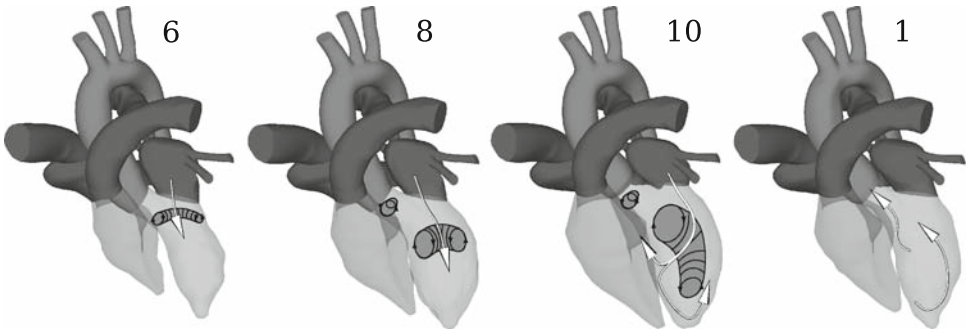

FIGURE 11. Schematic flow structure in the left ventricle. Numbering corresponds to the MRI flux phases (see Fig. 5).

DISCUSSION

The type of flow structure seen in our simulations (Fig. 10) corresponds to published experimental results[16,17] and from a physical point of view seems like an efficient way to ensure low losses and good flushing of the ventricle's elongated shape. To understand the complex interaction between the ventricular shape and its motion, the atrial flow or ventricular inflow conditions and the development of the initial ring cortex is crucial in the understanding of the hemodynamical function of the human heart.

As was shown in Long *et al.*[21] the intraventricular flow is highly dependent on the inflow boundary conditions.

Further validation of the complete numerical model and boundary condition is therefore indispensable. Since most of the discrepancy between numerical and *in vivo* measurement results cannot be clearly attributed to flaws in either the model itself or uncertainties in the measurement and segmentation an *in vitro* experiment has to be designed in order to validate the numerical model in full.

Our model does not include or simplifies several aspects of the ventricular function. We will discuss the expected impact on the validity of the simulation results briefly.

The representation of the valves used in the current study does not include any effect that the mitral valve leaflets could have on the flow. Nonetheless the agreement between the measured flow field and the simulated one shows no discrepancy in the valve area. This justifies the assumption that the healthy mitral valve leaflet does indeed orient itself in the flow and does not steer the flow or induce a tip vortex.

The error in the local radial velocity of the moving wall boundary is very high, since the velocities are low compared with the maximum spatial and temporal resolution of the MRI data. In addition we do not have any information on tangential velocity from the twisting motion of the ventricle. Nonetheless we think that the results can be used for this kind of simulation. The friction boundary layers resulting from the twisting motions are proportional to $\sqrt{\nu T/2}$, with T being the cycle length and therefore are at most a few millimeters thick and the bulk flow dominates. It seems that the twisting is not of fluid mechanical importance but of mechanical importance since twisting of the muscle highly increases the change of volume that can be realized from a given contraction. Furthermore we don't include the topology of the endocardium which is far from smooth, but cannot be resolved in the MRI. The fluid dynamical effect of the endocardium structure has not been studied. Also not included are the papillaries and trabeculae which will influence the flow field in the later diastole to the effect that they will increase the vortex breakdown.

The segmentation does not include the isovolumetric phases of the heart cycle, but we don't think that this is important for the development of the flow field. If the isovolumetric contraction is really isovolumetric it won't influence the flow in any way, since it will result in an increase in pressure only. In a real situation where the increase in pressure is not completely isovolumetric but results in a small contraction of the ventricle and a displacement of fluid toward the valvular plane combined with a bulging of the mitral valve this will definitely influence the vortex development due to the deceleration of the vortex which will increase vortex breakdown before systole begins. This might slightly effect the flow pattern for the systole.

In summary we think that the simplifications made in the model do not influence the development of the inlet vortex in a severe way so the results can be used to gain further insight into intraventricular flow. The effect of the simplifications, especially neglecting the dissipative effect of structures in the ventricle will increase further into the heart cycle.

CONCLUSION AND OUTLOOK

We have shown a three dimensional numerical model of the human left ventricular flow. The model is based on state of the clinical use MRI measurements and could therefore be used on a patient specific basis without putting additional stress on the patient. The model has been qualitatively validated by an overall comparison between the simulated data and velocity data obtained by additional flux measurement.

This study *per se* cannot be used for clinical purposes. Before any clinical claims can be made a full *in vitro* validation of the numerical model is necessary. But it does demonstrate the capabilities of state of the art CFD. In future such simulations could be used to extract quantities that cannot be assessed *in vivo*, like shear stresses, hemodynamic losses, and to derive parameters that can be used to evaluate the functionality of the ventricle, which could be used as indication whether or not medical intervention will be needed.

While the prospects are wide, we have also shown that the realistic prediction of the intraventricular flow pattern is only possible, if a correct representation for the atrial geometry can be included in the numerical model. It might therefore be necessary to extend the current MRI sequences to include the atrium. While the inclusion of the atrial geometry will pose other challenges with respect to the definition of proper boundary conditions, it will increase the overall fidelity of the numerical models and make it possible to predict

the intraventricular flow without generic adaption of the atrial representation. Further studies will have to show if this is a viable approach.

ACKNOWLEDGMENTS

The authors wish to thank all undergraduate, graduate and Ph.D. students that helped in developing the KaHMo. Especially we wish to thank Kathrin Spiegel who greatly simplified the tedious task of grid generation and Ron Schwarz from Fraunhofer FIT for the segmentation work.

REFERENCES

[1]Atkinson, D. J., and R. R. Edelman. Cineangiography of the heart in a single breath hold with a segmented turboflash sequence. *Radiology* 178:357–360, 1991.
[2]Axel, L. Blood flow effects in magnetic resonance imaging. *Am. J. Roentgenol.* 143(6):1157–1166, 1984.
[3]Baccani, B., F. Domenichini, and G. Pedrizzetti. Vortex dynamics in a model left ventricle during filling. *Eur. J. Mech. B/Fluids* 21:527–543, 2002.
[4]Baccani, B., F. Domenichini, and G. Pedrizzetti. Model and influence of mitral valve opening during the left ventricular filling. *J. Biomech.* 36:355–361, 2003.
[5]Baccani, B., F. Domenichini, G. Pedrizzetti, and G. Tonti. Fluid dynamics of the left ventricular filling in dilated cardiomyopathy. *J. Biomech.* 35(5):665–671, 2002.
[6]Bolzon, G., L. Zovatto, and G. Pedrizzetti. Birth of three-dimensionality in a pulsed jet through a circular orifice. *J. Fluid Mech.* 493:209–218, 2003.
[7]Chahboune, B., and J. M. Crolet. Numerical simulation of the blood-wall interaction in the human left ventricle. *Eur. Phys. J. Appl. Phys.* 2:291–297, 1998.
[8]Cheng, Y., H. Oertel, and T. Schenkel. Fluid–structure coupled cfd simulation of the left ventricular flow during filling phase. *Ann. Biomed. Eng.* 33(5):567–576, 2004.
[9]Domenichini, F., G. Pedrizzetti, and B. Baccani. Three-dimensional filling flow into a model left ventricle. *J. Fluid Mech.* 539:179–198, 2005.
[10]Ebbers, T., L. Wigstrï, A. F. Bolger, B. Wranne, and M. Karlsson. Noninvasive measurement of time-varying three-dimensional relative pressure fields within the human heart. *J. Biomech. Eng.* 124:288–293, 2002.
[11]Ferziger, J., and M. Peric. Computational Methods for Fluid Dynamics. Berlin: Springer, 1997.
[12]Geiger, D., A. Gupta, L. A. Costa, and J. Vlontzos. Dynamic programming for detection, tracking and matching deformable contours. *IEEE Trans. PAMI* 17(3):294–302, 1995.
[13]Hennig, J. K-space sampling strategies. *Eur. Radiol.* 9:1020–1031, 1999.
[14]Hunter, P. J., A. J. Pullan, and B. H. Smaill. Modeling total heart function. *Annu. Rev. Biomed. Eng.* 5:147–177, 2003.
[15]Jolly, M.-P. Combining edge, region and shape information to segment the left ventricle in cardiac mr images. In: MICCAI, 2001, pp. 482–490.
[16]Kilner, P. J., G.-Z. Yang, A. J. Wilkes, R. H. Mohiaddin, D. N. Firmin, and M. H. Yacoub. Asymmetric redirection of flow through the heart. *Nature* 404:759–761, 2000.
[17]Kim, W. Y., P. G. Walker, E. M. Pedersen, J. K. Poulsen, S. Oyre, K. Houlind, and A. P. Yoganathan. Left ventricular blood flow patterns in normal subjects: a quantitative analysis by three-dimensional magnetic resonance velocity mapping. *JACC* 26(1):224–238, 1995.
[18]Lemmon, J. D., and A. P. Yoganathan. Computational modeling of left herat diastolic function: examination of ventricluar dysfunction. *J. Biomech. Eng.* 122:297–303, 2000.
[19]Lemmon, J. D., and A. P. Yoganathan. Three-dimensional computational model of left heart diastolic function with fluid–structure interaction. *J. Biomech. Eng.* 122:109–117, 2000.
[20]Lima, J. A., and M. Y. Desai. Cardiovascular magnetic resonance imaging: current and emerging applications. *J. Am. Coll. Cardiol.* 44(6):1164–1171, 2004.
[21]Long, Q., R. Merrifield, G. Z. Yang, X. Y. Xu, P. J. Kilner, and D. N. Firmin. The influence of inflow boundary conditions on intra left ventricle flow predictions. *J. Biomech. Eng.* 125:922–927, 2003.
[22]Lorenz, C. H., E. S. Walker, V. L. Morgan, S. S. Klein, and T. P. Graham, Jr. Normal human right and left ventricular mass, systolic function, and gender differences by cine magnetic resonance imaging. *J. Cardiovasc. Magn. Reson.* 1:7–21, 1999.
[23]McQueen, D. M., and C. Peskin. Shared-memory parallel vector implementation of the immersed boundary method for the computation of blood flow in the beating mammalian heart. *J. Supercomput.* 11(3):213–236, 1997.
[24]McQueen, D. M., and C. Peskin. A three-dimensional computer model of the human heart for studying cardiac fluid dynamics. *Comput. Graph.* 34:56–60, 2000.
[25]Mortensen, E. N., and W. A. Barrett. Interactive segmentation with intelligent scissors. *Graph. Models Image Process.* 60(5):349–384, 1998.
[26]Nakamura, M., S. Wada, T. Mikami, A. Kitabatake, and T. Karino. Computational study on the evolution of an intraventricular vortical flow during early diastole for the interpretation of color m-mode doppler echocardiogramms. *Biomech. Model. Mechanobiol.* 2:59–72, 2003.
[27]Nash, M. P., and P. J. Hunter. Computational mechanics of the heart: from tissue structure to ventricular function. *J. Elast.* 61(1/3):113–141, 2000.
[28]Naujokat, E., and U. Kiencke. Neuronal and hormonal cardiac control processes in a model of the human circulatory system. *Int. J. Bioelectromagn.* 2(2), 2000.
[29]Noble, D. Modelling the heart: from genes to cells to the whole organ. *Science* 295:1678–1682, 2002.
[30]Pedrizzetti, G., and F. Domenichini. Nature optimizes the swirling flow in the human left ventricle. *Phys. Rev. Lett.* 95:108101, 2005.
[31]Pelc, N. J., R. J. Herfkens, A. Shimakawa, and D. R. Enzmann. Phase contrast cine magnetic resonance imaging. *Magn. Reson. Q.* 7(4):229–254, 1991.
[32]Perktold, K., M. Prosi, and H. Florian. Computational models of arterial flow and mass transport. *CISM Courses Lect.* 446:73–136, 2003.
[33]Peskin, C. S., and D. M. McQueen. Fluid dynamics of the heart and its valves, case studies in mathematical modeling, In: Ecology, Physiology and Cell Biology. New Jersey: Pretice-Hall, 1996, pp. 309–337.

[34]Rebergen, S. A., E. E. van der Wall, J. Doornbos, and A. de Roos. Magnetic resonance measurement of velocity and flow: technique, validation, and cardiovascular applications. *Am. Heart J*. 126(6):1439–1456, 1993.

[35]Saber, N. R., A. D. Gosman, N. B. Wood, P. J. Kilner, C. L. Charrier, and D. N. Firmin. Computational flow modeling of the left ventricle based on *in vivo* mri data: Initial experience. *Ann. Biomed. Eng*. 29(4):275–283, 2001.

[36]Saber, N. R., N. B. Wood, A. D. Gosman, R. D. Merrifield, G. Z. Yang, C. L. Charrier, P. D. Gatehouse, and D. N. Firmin. Progress towards patient-specific computational flow modeling of the left heart via combination of magnetic resonance imaging with computational fluid dynamics. *Ann. Biomed. Eng*. 31(1):42–52, 2003.

[37]Schenk, A., G. Prause, and H. Peitgen. Local cost computation for efficient segmentation of 3d objects with live wire. In: Proceedings of SPIE, edited by M. Sonka and K. M. Hanson. SPIE, Vol. 4322, 2001, pp. 1357–1364.

[38]Schoephoerster, R. T., C. L. Silva, and G. Ray. Evaluation of ventricular function based on simulated systolic flow dynamics computed from regional wall motion. *J. Biomech*. 27:125–136, 1994.

[39]Stalling, D., and H.-C. Hege. Intelligent scissors for medical image segmentation. In: Tagungsband zum 4. Freiburger Workshop: Digitale Bildverarbeitung in der Medizin, edited by B. Arnolds, H. Mueller, T. Saupe, and D. Tolxdorf, 1996, pp. 32–36.

[40]Taylor, T. W., H. Okino, and T. Yamaguchi. Three-dimensional analysis of left ventricular ejection using computational dynamics. *J. Biomech. Eng*. 116:127–130, 1994.

[41]Vesier, C., J. D. Lemmon, R. A. Levine, and A. P. Yoganathan. A three-dimensional computational model of a thin-walled left ventricle. In: Proceedings on IEEE Supercomputing '92, 16–20 November, 1992, pp. 73–82.

[42]Vierendeels, J. A., K. Riemslagh, and E. Dick. Computer simulation of intraventricular flow and pressure gradients during diastole. *J. Biomech. Eng*. 122:667–674, 2000.

[43]Vierendeels, J. A., K. Riemslagh, E. Dick, and P. Verdonck. Computer simulation of left ventricular filling flow. *Comput. Cardiol*. 26:177–180, 1999.

[44]Watanabe, H., T. Hisada, S. Sugiura, J. Okada, and H. Fukunari. Computer simulation of blood flow, left ventricular wall motion and their interrelationship by fluid–structure interaction finite element method. *JSME Int. J. Ser. C- Mech. Syst. Mach. Elem. Manufact*. 45(4):1003–1012, 2002.

[45]Watanabe, H., S. Sugiura, H. Kafuku, and T. Hisada. Multiphysics simulation of left ventricular filling dynamics using fluid–structure interaction finite element method. *Biophys. J*. 87:2074–2085, 2004.